Available online at www.sciencedirect.com
ScienceDirect
Scripta Materialia 65 (2011) 656–659
Scripta MATERIALIA
www.elsevier.com/locate/scriptamat

Towards atomic scale engineering of rare-earth-doped SiAlON ceramics through aberration-corrected scanning transmission electron microscopy

Hilmi Yurdakul,[a,b] Juan C. Idrobo,[b,c] Stephen J. Pennycook[b,c] and Servet Turan[a,*]

[a]Department of Materials Science and Engineering, Anadolu University, Eskisehir, TR-26480, Turkey
[b]Materials Science and Technology Division, Oak Ridge National Laboratory, Oak Ridge, TN 37831, USA
[c]Department of Physics and Astronomy, Vanderbilt University, Nashville, TN 37235, USA

Received 2 June 2011; revised 26 June 2011; accepted 27 June 2011
Available online 1 July 2011

Direct visualization of rare earths in α- and β-SiAlON unit-cells is performed through *Z*-contrast imaging technique in an aberration-corrected scanning transmission electron microscope. The preferential occupation of Yb and Ce atoms in different interstitial locations of β-SiAlON lattice is demonstrated, yielding higher solubility for Yb than Ce. The triangular-like host sites in α-SiAlON unit cell accommodate more Ce atoms than hexagonal sites in β-SiAlON. We think that our results will be applicable as guidelines for many kinds of rare-earth-doped materials.
© 2011 Acta Materialia Inc. Published by Elsevier Ltd. All rights reserved.

Keywords: Ceramics; Rare earth; Scanning transmission electron microscope (STEM); SiAlON, *Z*-contrast microscopy

SiAlON ceramics are of major interest for industrial applications due to their improved mechanical and optical properties compared to their parent silicon nitride (Si_3N_4) compounds [1–6]. The improved performance is facilitated by the ability of the material to accept dopant atoms in the bulk with respect to Si_3N_4 ceramics [7–9]. SiAlONs are formed by sintering at high temperatures, when a rare-earth-rich liquid intergranular phase facilitates development of a high-density microstructure [2,10]. However, as the sample cools, the rare-earth sintering dopants must be absorbed by the bulk to achieve good high-temperature mechanical and optical properties [11–14]. The outstanding properties of SiAlONs are due to the presence of substituted O and Al atoms in α- and β-Si_3N_4 lattices, which offer a variety of different favorable sites for dopant rare-earth atoms [1,7–9,15,16], allowing both α- and β-SiAlONs to be stabilized to optimize the hardness, fracture toughness and luminescence [11–14]. In general, the rare earths with large atomic numbers ($Z \geqslant 60$, with the exception of Eu) enhance the stability and hardness of the α-SiAlON phase, while those with smaller atomic numbers ($Z \leqslant 60$) increase the fracture toughness of the β-SiAlON phase and also contribute to $\alpha \rightarrow \beta$ phase transformation during the sintering process [17]. Additionally, depending on the type of rare-earth element used for densification, SiAlON ceramics show novel optical properties [13,18,19], which also make them a relatively cheap and promising material for the next generation of white light-emitting diodes (LEDs) [5,6]. Hence there are widespread potential industrial applications for SiAlON ceramics, but the key factor missing to realize this potential is to atomically understand and control where and how much rare earths can be incorporated into the α- and β-SiAlON lattices.

In the present research, we have used *Z* (atomic number)-contrast imaging [20] in an aberration-corrected scanning transmission electron microscope (STEM) to directly visualize the atomic locations of rare-earth atoms in α- and β-SiAlON unit cells, from which we are able to quantify the solubility concentrations. The experimental section is described in the Supporting Information.

First, we studied a SiAlON sample sintered with an additive composition of 8 wt.% CeO_2. X-ray diffraction analysis indicates that the sintered sample has an α-phase of ~4% (Fig. S1a of the Supporting Information), which agrees with the few previous microscale studies

* Corresponding author. Tel.: +90 222 3213550x6356; fax: +90 222 3239501; e-mail: sturan@anadolu.edu.tr

1359-6462/$ - see front matter © 2011 Acta Materialia Inc. Published by Elsevier Ltd. All rights reserved.
doi:10.1016/j.scriptamat.2011.06.038

showing that Ce may stabilize the α-phase when it is used alone [21,22].

Figure 1a shows an atomically resolved *Z*-contrast image of a typical region of a β-SiAlON grain oriented along the [0 0 0 1] zone axis. We find that a number of small areas (~2 Å in diameter) close to the center of some of the hexagons, which consist of Si(Al) and N(O) atomic columns, have peak intensities that are above the background noise (positions highlighted with white arrows in Fig. 1a). The unexpectedly high intensity observed in some places around the center of the hexagons can be better observed after performing a maximum entropy deconvolution [23] on the experimental image in Figure 1b, and by comparing corresponding intensity profiles obtained from the crystallographically identical "A", "B" and "C" atomic sites in Figure 1c. The reason for the surprising excess intensity in some hexagons is attributed to interstitial Ce atoms. Similar to our observation, it has been reported previously that Eu impurities occupy equivalent positions in β-SiAlON [24]. However, in the case of our experiment, the direct imaging of Ce atoms within the hexagons immediately shows that the Ce interstitials are more abundant than the Eu interstitials [24]. Therefore, this atomic-scale finding brings support to the belief, suggested in a non-microscopic study [25], that Ce may also be incorporated into the hexagon sites with a larger solubility than Eu in β-SiAlON [25].

In addition, we quantified the intensity of numerous interstitial atomic sites where the Ce is observed in Figure 1a. We find that the intensity of the Ce atoms within the hexagons is statistically similar (Fig. S2(a–d) of the Supporting Information). This result, and the fact that many sites are observed without Ce, implies that the Ce atoms are present as single interstitial atoms at the thicknesses studied.

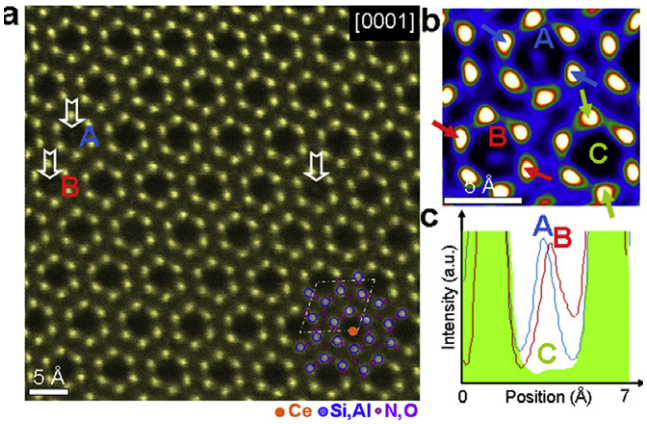

Figure 1. (a) *Z*-contrast image (raw data) of β-SiAlON:Ce in the [0 0 0 1] crystallographic orientation. White arrows indicate the positions where interstitial Ce atoms can be observed. Superimposed is a model β-SiAlON crystal structure including the Ce interstitial; the unit cell is shown by a dashed parallelogram. (b) Maximum entropy deconvolution image obtained from a region surrounding "A" and "B" in (a). (c) Intensity line profiles obtained along the directions highlighted by the red, green and blue arrows shown in (b). The empty C interstitial location is crystallographically identical to the occupied sites. (For interpretation of the references to color in this figure legend, the reader is referred to the web version of this article.)

Figure 2a shows an atomically resolved *Z*-contrast image of a typical region of an α-SiAlON grain oriented along the [0 0 0 1] zone axis. Similar to the β-SiAlON grains, we also find interstitial Ce atoms in the α-SiAlON grains (highlighted by white arrows in Fig. 2a). Again, the interstitial Ce atoms can be better observed after performing a maximum entropy deconvolution analysis in Figure 2b. Furthermore, intensity profiles obtained from some positions with (D) and without (E) Ce atoms are shown in Figure 2c. Based on the results reported in Figure 2a–c, we conclude that the Ce atoms are located at the center of the triangular-like interstitial sites in α-SiAlON structure. Here, direct observation of Ce atoms within the α-SiAlON unit cell runs counter to the common belief, strongly supported by some previous microscale studies [26–33], that the α-SiAlON phase cannot be stabilized by Ce alone without using a co-sintering cation such as Y [26–31] or the addition of Y-α-SiAlON nuclei [32,33]. Instead, our observation reveals definitive atomic-scale evidence for Ce stability in the α-SiAlON lattice when it is used alone, in agreement with other previous microscale observations [21,22].

A simple visual inspection of the acquired *Z*-contrast image reveals that the intensity of the Ce impurities is not constant and changes significantly from site to site. This finding is also supported by the quantified intensity of interstitial Ce atoms in the α-SiAlON crystal structure (Fig. S3(a–d) of the Supporting Information). The variation in intensity corresponds to multiple Ce atoms in the same projected channel location, and is consistent with the much higher fractional occupation of the interstitial sites.

Next, we sintered a SiAlON sample with an additive composition of 8 wt.% Yb_2O_3. The X-ray diffraction analysis reveals that the sintered sample consists of 100% β-SiAlON phase (Fig. S1b of the Supporting Information), which contradicts previous studies

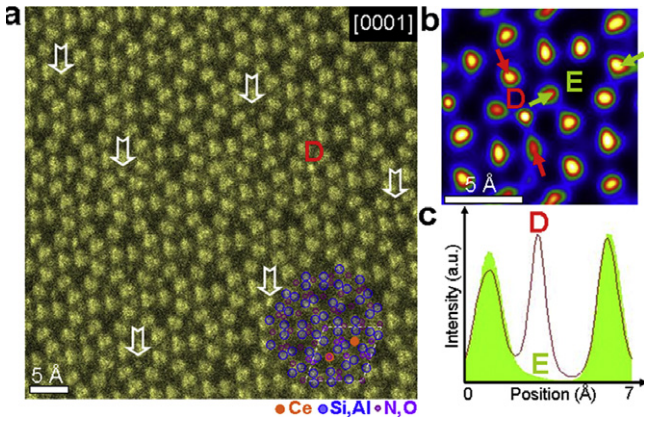

Figure 2. (a) *Z*-contrast image (raw data) of α-SiAlON:Ce in the [0 0 0 1] crystallographic orientation with superimposed structure. White arrows indicate the positions where interstitial Ce atoms can be observed. (b) Maximum entropy deconvolution image obtained from a region surrounding "D" in (a). (c) Intensity line profiles obtained along the directions highlighted by the red and green arrows shown in (b). The empty E interstitial location is crystallographically identical to the occupied sites. (For interpretation of the references to color in this figure legend, the reader is referred to the web version of this article.)

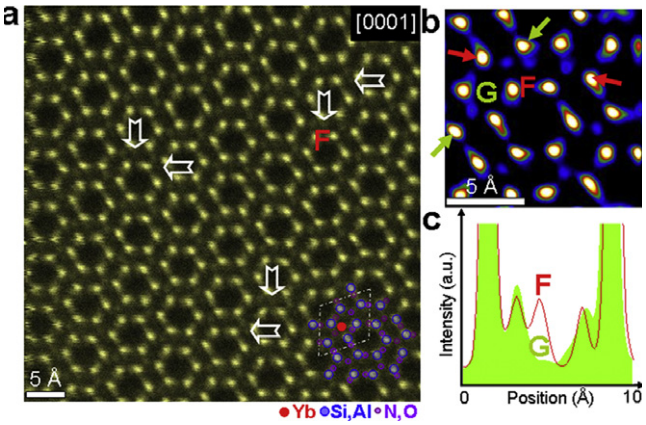

Figure 3. (a) *Z*-contrast image (raw data) of β-SiAlON:Yb in the [0 0 0 1] crystallographic orientation with superimposed structure. White arrows indicate the positions where interstitial Yb atoms can be observed. (b) Maximum entropy deconvolution image obtained from a region surrounding "F" in (a). (c) Intensity line profiles obtained along the directions highlighted by the red and green arrows shown in (b). The empty G interstitial location is crystallographically identical to the occupied sites. (For interpretation of the references to color in this figure legend, the reader is referred to the web version of this article.)

reporting that rare earths with atomic number larger than 60 (except Eu) easily stabilize the α-phase after sintering [34,35].

Figure 3a shows an atomically resolved *Z*-contrast image of a typical region of a β-SiAlON grain oriented along the [0 0 0 1] zone axis. A maximum entropy deconvolution image is shown in Figure 3b, with corresponding intensity profiles obtained from crystallographically identical "F" and "G" atomic sites in Figure 3c. Considering the results in Figure 3a–c, similar to the Ce-sintered β-SiAlON sample, the Yb-sintered β-SiAlON sample also unexpectedly presents Yb interstitial atoms. However, the Yb interstitial sites are not equivalent to the Ce interstitial sites. Yb atoms sit in between two adjacent hexagons (as highlighted by the white arrows in Fig. 3a), while Ce atoms sit at interstitial positions that are located around the center of the hexagon rings (see Fig. 1a). Our atomic-scale observations show that Yb is preferentially absorbed into a new interstitial site of the β-SiAlON lattice with respect to Ce or Eu [24]. The result suggests that Yb ($Z = 70$) can promote a complete $\alpha \rightarrow \beta$ phase transformation in SiAlON ceramics due to the slow cooling of the furnace to room temperature during the sintering process [36].

We also quantified the intensity of the interstitial atomic sites where the Yb is observed in β-SiAlON. We found that the intensity of the Yb atoms within this new interstitial site is not constant but changes from site to site (Fig. S4(a–e) of the Supporting Information). As with the case of Ce, this result again implies that multiple Yb atoms are being imaged along the [0 0 0 1] crystallographic direction, which is again consistent with the concentration.

From the experimental images we were able to quantify the concentrations of interstitial Ce atoms in both the α- and β-SiAlON phases and Yb atoms in the β-SiAlON phase. The quantification was performed by simply counting the number of interstitial atoms observed in the experimental images per unit area (the detailed quantification procedure is described in the Supporting Information). We found that only 3% of the β-SiAlON unit cells have interstitial Ce atoms, while for the α-SiAlON the concentration of Ce atoms reaches 49%. In contrast, the calculated concentration of Yb atoms in β-SiAlON reaches 69%. Using the measured concentrations, we estimate that the volume fractions are $0.35 \pm 0.02\%$ and $0.015 \pm 0.002\%$ for Yb and Ce in β-SiAlON, respectively, and $0.45 \pm 0.01\%$ for Ce in α-SiAlON. Here, these error bars represent only the statistical error bars based on the number of interstitials observed. They do not take account of any beam broadening, which may cause interstitials lying deep inside the crystal to be out of focus and therefore invisible. For this reason, the quoted concentrations represent an upper limit.

In conclusion, the precise sites of Ce and Yb rare-earth atoms within α- and β-SiAlON crystal structures after sintering were determined using an aberration-corrected STEM. We find that Yb and Ce atoms preferentially locate in different interstitial lattice sites in the β-SiAlON crystal structure, with an order of magnitude higher solubility for Yb than for Ce. The result clearly shows that some sintering additives, like Yb and Ce, can be incorporated into the β-SiAlON crystal structure during sintering. We observe that Ce atoms are located at the triangular-like interstitial sites in α-SiAlON crystal structure. Furthermore, we find that absorption of Ce atoms in the α-SiAlON lattice is higher than in the β-SiAlON lattice.

Our results demonstrate that direct visualization of the atomic sites and solubility of rare-earth atoms in α- and β-SiAlON crystal structures is possible. This capability offers new atomic-level engineering insights into how appropriate rare-earth types and host SiAlON polymorphs should be chosen for nanoscopic tailoring of both next-generation SiAlON-based structural materials and optical ceramics. In particular, we have shown that if Yb, the best-known microscale α-phase stabilizer [34,35], is utilized to produce SiAlON-based ceramic cutting tools, fast cooling is essential to prevent the $\alpha \rightarrow \beta$ phase transformation from occurring, which is not practical for industrial applications. On the other hand, we have shown that Ce, which has not so far been considered as an α-phase stabilizer [26–33], does have the ability to stabilize α-SiAlON without any co-dopant [26–31] or α-nuclei additive [32,33]. SiAlON polymorphs are also promising host crystals for LED technologies [37–40]. Based on our observations, if β-SiAlON is activated by Yb or Ce [41], we might anticipate Yb to have the higher luminescence efficiency due to its higher solubility. On the other hand, if Ce is required as a dopant, then α-SiAlON would be a better choice of host crystal lattice since the solubility of Ce in α-SiAlON lattice is much higher than in β-SiAlON.

We therefore expect our first observations of impurity sites and solubilities in SiAlON polymorphs to represent the first step towards a new paradigm for atomic-scale guidance in the production of rare-earth-doped materials for a wide variety of applications.

This research was supported by The Scientific and Technological Research Council of Turkey (TUBITAK) through 2214-International Doctoral Research Fellowship Program (H.Y.), by National Science Foundation through Grant No. DMR-0605964 (J.C.I.), Oak Ridge National Laboratory's SHaRE User Facility (J.C.I.), which is sponsored by the Office of Basic Energy Sciences, US Department of Energy, and the Office of Basic Energy Sciences, Materials Sciences and Engineering Division, US Department of Energy (S.J.P.). We also would like to thank MDA Advanced Ceramics (Eskisehir, Turkey) for the provision of the samples produced from the project with a contract number of 3040287 - Technology and Innovation Funding Programmes Directorate (TEYDEB), Turkey.

Supplementary data associated with this article can be found, in the online version, at doi:10.1016/j.scriptamat.2011.06.038.

[1] K.H. Jack, J. Mater. Sci. 11 (1976) 1135–1158.
[2] S. Hampshire, J. Achiev. Mater. Manu. Engin. 24 (2007) 43–50.
[3] V.A. Izhevskiy, L.A. Genova, J.C. Bressiani, F. Aldinger, J. Eur. Ceram. Soc. 20 (2000) 2275–2295.
[4] F.L. Riley, J. Am. Ceram. Soc. 83 (2000) 245–265.
[5] R.J. Xie, N. Hirosaki, M. Mitomo, J. Electroceram. 21 (2008) 370–373.
[6] R.J. Xie, N. Hirosaki, Sci. Tech. Adv. Mater. 8 (2007) 588–600.
[7] S. Hampshire, H.K. Park, D.P. Thompson, K.H. Jack, Nature 274 (1978) 880–882.
[8] T. Nakayasu, T. Yamada, I. Tanaka, H. Adachi, S. Goto, J. Am. Ceram. Soc. 79 (1996) 2527–2532.
[9] T. Nakayasu, T. Yamada, I. Tanaka, H. Adachi, S. Goto, J. Am. Ceram. Soc. 80 (1997) 2525–2532.
[10] D.P. Thompson, Nature 417 (2002) 237.
[11] H. Mandal, J. Eur. Ceram. Soc. 19 (1999) 2349–2357.
[12] I.W. Chen, A. Rosenflanz, Nature 389 (1997) 701–704.
[13] B.S.B. Karunaratne, R.J. Lumby, M.H. Lewis, J. Mater. Res. 11 (1996) 2790–2794.
[14] N. Hirosaki, R.J. Xie, K. Kimoto, T. Sekiguchi, Y. Yamamoto, T. Suehiro, M. Mitomo, Appl. Phys. Lett. 86 (2005) 211905.
[15] D.P. Thompson, Mater. Sci. For. 47 (1989) 21–42.
[16] S.V. Okatov, A.L. Ivanovskii, Phys. Stat. Sol. (b) 231 (2002) R11-R13.
[17] H. Mandal, F. Kara, S. Turan, A. Kara, U.S. Patent Appl. (2004) Pub. No. US2004/0067838 A1.
[18] W.W. Chen, Y.B. Cheng, P.I. Wang, D.S. Yan, Key Eng. Mater. 264–286 (2004) 905.
[19] M.I. Jones, J. Am. Ceram. Soc. 87 (2004) 714–716.
[20] S.J. Pennycook, B. Rafferty, P.D. Nellist, Microsc. Microanal. 6 (2000) 343–352.
[21] H. Mandal, D.P. Thompson, J. Mater. Sci. Lett. 15 (1996) 1435–1438.
[22] Z. Shen, M. Nygren, J. Eur. Ceram. Soc. 21 (2001) 611–615.
[23] J.J. Hu, F.H. Li, Ultramicroscopy 35 (1991) 339–350.
[24] K. Kimoto, R.J. Xie, Y. Matsui, K. Ishizuka, N. Hirosaki, Appl. Phys. Lett. 94 (2009) 041908.
[25] L.H. Liu, R.J. Xie, N. Hirosaki, T. Takeda, C.N. Zhang, J.G. Li, X.D. Sun, J. Electrochem. Soc. 157 (2010) H50–H54.
[26] P.O. Olsson, J. Mater. Sci. 24 (1989) 3878–3887.
[27] E. Söderlund, T. Ekström, J. Mater. Sci. 25 (1990) 4815–4821.
[28] T. Ekström, K. Jansson, P.O. Olsson, J. Persson, J. Eur. Ceram. Soc. 8 (1991) 3–9.
[29] J.X. Jiang, P.L. Wang, W.B. He, W.W. Chen, H.R. Zhuang, Y.B. Cheng, D.S. Yan, Mater. Lett. 58 (2004) 3266–3270.
[30] J.X. Jiang, P.L. Wang, W.B. He, W.W. Chen, H.R. Zhuang, Y.B. Cheng, D.S. Yan, J. Eur. Ceram. Soc. 24 (2004) 2853–2860.
[31] J.X. Jiang, P.L. Wang, W.B. He, W.W. Chen, H.R. Zhuang, Y.B. Cheng, D.S. Yan, J. Am. Ceram. Soc. 87 (2004) 703–705.
[32] C.M. Wang, M. Mitomo, F.F. Xu, N. Hirosaki, Y. Bando, J. Am. Ceram. Soc. 84 (2001) 1389–1391.
[33] F.F. Xu, Y. Bando, C.M. Wang, M. Mitomo, J. Am. Ceram. Soc. 85 (2002) 466–472.
[34] Z. Shen, M. Nygren, J. Eur. Ceram. Soc. 17 (1997) 1639–1645.
[35] A. Rosenflanz, I.W. Chen, J. Am. Ceram. Soc. 82 (1999) 1025–1036.
[36] H. Mandal, J. Am. Ceram. Soc. 82 (1999) 229–232.
[37] R.J. Xie, N. Hirosaki, M. Mitomo, K. Uheda, T. Suehiro, X. Xu, Y. Yamamoto, T. Sekiguchi, J. Phys, Chem. B 109 (2005) 9490–9494.
[38] B. Dierre, X.L. Yuan, N. Hirosaki, T. Kimura, R.J. Xie, T. Sekiguchi, J. Mater. Res. 23 (2008) 1701–1705.
[39] J.W.H. van Krevel, J.W.T. van Rutten, H. Mandal, H.T. Hintzen, R. Metselaar, J. Solid. State. Chem. 165 (2002) 19–24.
[40] R.J. Xie, N. Hirosaki, M. Mitomo, Y. Yamamoto, T. Suehiro, N. Ohashi, J. Am. Ceram. Soc. 87 (2004) 1368–1370.
[41] J.H. Ryu, H.S. Won, Y.G. Park, S.H. Kim, W.Y. Song, H. Suzuki, C.B. Yoon, D.H. Kim, W.J. Park, C. Yoon, Electrochem. Solid-State Lett. 13 (2010) H30–H32.